JPE 13-3-1

http://dx.doi.org/10.6113/JPE.2013.13.3.329

Analysis of the Charging Characteristics of High Voltage Capacitor Chargers Considering the Transformer Stray Capacitance

Byungha Lee* and Hanju Cha†

*Defense Advanced R&D Institute, Agency for Defense Development, Daejeon, Korea
†Dept. of Electrical Engineering, Chungnam National University, Daejeon, Korea

Abstract

In this paper, the charging characteristics of series resonant type high voltage capacitor chargers considering the transformer stray capacitance have been studied. The principles of operation for the four operational modes and the mode changes for the four different switching frequency sections are explained and analyzed in the range of switching frequency below the resonant frequency. It is confirmed that the average charging currents derived from the above analysis results have non-linear characteristics in each of the four modes. The resonant current, resonant voltage, charging current, and charging time of this capacitor charger as variations of the switching frequency, series parallel capacitance ratio ($k=C_p/C_s$), and output voltage are calculated. From the calculation results, the advantages and disadvantages arising from the parallel connection of this stray capacitance are described. Some methods to minimize charging time of this capacitor charger are suggested. In addition, the results of a comparative test using two transformers whose stray capacitances are different are described. A 1.8 kJ/s prototype capacitor charger is assembled with a TI28335 DSP controller and a 40 kJ, 7 kV capacitor. The analysis results are verified by the experiment.

Key words: Capacitor charger, Series-parallel resonant converter, Transformer stray capacitance

I. INTRODUCTION

In the military pulsed power system of an Electromagnetic Launcher (EML) or Electromagnetic Armor (EMA), the capacitor bank is the most commonly used energy storage equipment because of its advantages in regards to operability, cost, ease of pulse forming, expandability and maintenance [1], [2]. The pulsed power system of an EML is composed of several paralleled segments whose capability is hundreds of kJ ~ MJ. The capacitor charger which charges this capacitor bank is requisitely installed in each segment [2]-[4] where its high efficiency, high reliability, high power density, fast charging capability are simultaneously required. Although high power capacitor chargers have often been implemented through PWM topologies [5], [6], resonant topologies have been preferred to PWM topologies because the resonant topologies operate advantageously under various load conditions such as shorts or open circuit [7]-[9]. Among the various resonant topologies, the series resonant type topology which has a simple circuit, constant characteristic impedance and constant resonant frequency even in a wide range of load capacitances has been adopted more often for high voltage and high power capacitor chargers [10]-[14]. In the series resonant capacitor chargers for EMLs, a high output voltage above 10 kV is generally required. Accordingly, many turns in the secondary side of the transformer are needed, and a non-negligible stray capacitance arises from many turns in the secondary side. A capacitance which is proportional to the square of the secondary turns is connected to the series resonant capacitance in the primary side in parallel. Consequently, the ideal series resonant charging characteristic disappears and the series-parallel resonant charging characteristic appears as the output voltage increases. As a result, the charging time taken to reach a target voltage increases in comparison with the ideal series resonant type chargers. In a recent study regarding series resonant type chargers, a charging time error

Manuscript received Nov. 7, 2012; revised Feb. 19, 2013
Recommended for publication by Associate Editor Sangshin Kwak.
†Corresponding Author: hjcha@cnu.ac.kr
Tel: +82-42-821-7006, Fax: +82-42-821-8895, Chungnam Nat'l Univ.
*Defense Advanced R&D Inst., Agency for Defense Development, Korea

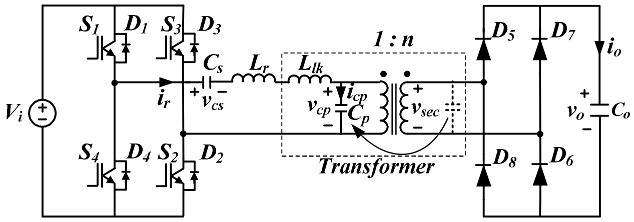

Fig. 1. Power circuit of series resonant type capacitor charger considering the transformer stray capacitance.

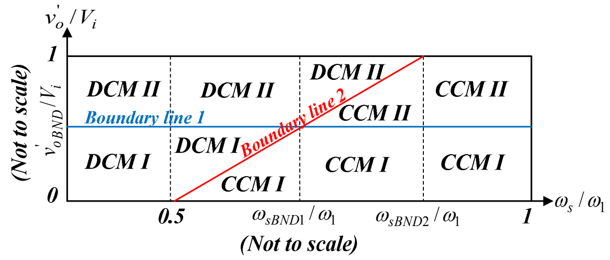

Fig. 2. Mode change by switching frequency section ($\omega_s < \omega_1$).

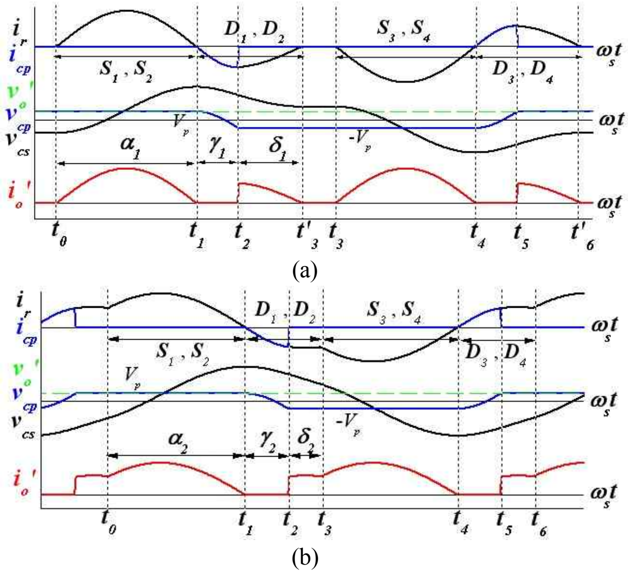

Fig. 3. Ideal waveforms of proposed capacitor charger. (a) DCM I. (b) CCM I.

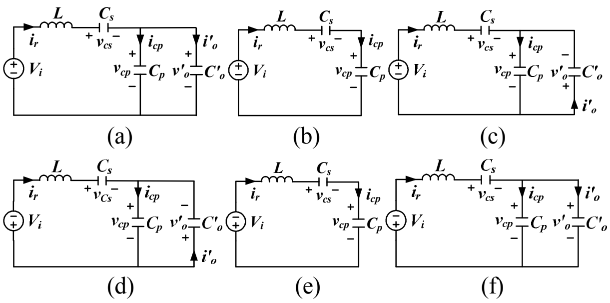

Fig. 4. Common equivalent circuit of DCM I and CCM I. (a) Mode 1. (b) Mode 2. (c) Mode 3. (d) Mode 4. (e) Mode 5. (f) Mode 6.

was found between the design and the experiment [15]. In this paper, the charging characteristics of series resonant type high voltage capacitor chargers considering the transformer stray capacitance is studied in detail. When this charger is operated in the switching frequency range below the resonant frequency, the principles of operation include four operational modes. Discontinuous conduction mode I (DCM I), continuous conduction mode I (CCM I), discontinuous conduction mode II (DCM II), and continuous conduction mode II (CCM II) are explained and analyzed. The mode changes in terms of the four different frequency sections are explained and the average charging currents for the four operation modes are derived. According to variations of the switching frequency, series parallel capacitance ratio ($k=C_p/C_s$) and output voltage, the charging characteristics are analyzed in terms of the normalized peak resonant current, normalized peak resonant voltage and charging time. A 1.8 kJ/s prototype capacitor charger is constructed and analyzed. The analysis results are verified by the experiment.

II. Analysis of High Voltage Capacitor Chargers

Fig. 1 shows a full bridge series resonant type capacitor charger with a capacitor load. Here, the parasitic resistance of the circuit is neglected. All of the switches and diodes are considered ideal. The secondary winding capacitance of the transformer, which is converted to the primary side C_p, acts as an additional resonant component. The resonant inductance L is the sum of the equivalent leakage inductance of the transformer L_{lk} and the inserted resonant inductance L_r. C_s is the inserted series capacitance and C_o is the capacitance of the high voltage output capacitor. n is the turns ratio of the transformer. This capacitor charger can be operated both below and above the system resonant frequency ω_1. However, in a high power capacitor charger, it is advantageous to operate below the resonant frequency and to use the IGBT as the main switching device because the switching loss can be minimized by zero-current turn-off. In this capacitor charger, the charging characteristic can be classified into four frequency sections, as shown in Fig. 2. The four operational modes (DCM I, CCM I, DCM II, and CCM II) are combined by each frequency section. Boundary line 1 divides the double pulse current (DPC) output mode and the single pulse current (SPC) output mode. Boundary line 2 divides the DCM and the CCM. The level of boundary line 1, the shape of boundary line 2, and the position of the boundary frequencies (ω_{sBND1}, ω_{sBND2}) are fully changed by the k value. The four operational modes (DCM I, CCM I, DCM II, and CCM II) are again divided into six operation modes (Mode 1~Mode 6) depending on the conduction paths of $S_1 \sim S_4$ and $D_1 \sim D_4$. In DCM I and DCM II, there exists an additional discontinuous section where all of the switches and diodes are not conductive.

A. Principles of Operation in DCM I and CCM I

Fig. 3 (a) and (b) show ideal waveforms in DCM I and in CCM I. Fig. 4 shows the equivalent circuits for the six operation modes which commonly appear in DCM I and CCM I.

In *Mode 1* [t_0-t_1], S_1 and S_2 are conductive and the positive resonant current i_r charges C_s. Meanwhile, v_{cs} increases. i_r is divided into i_{cp} and i'_o. i_{cp} charges C_p. i'_o charges C'_o since D_5 and D_6 are conductive. Both v_{cp} and v'_o increase. Here, v_{cp} is equal to v'_o. Because i_{cp} is much smaller than i_r, v_{cp} has a relatively small increases in comparison with v_{cs}. S_1 and S_2 are naturally turned off at $t = t_1$ and zero current switching (ZCS) is achieved. The currents i_r, i_{cp}, i'_o and the voltages v_{cs}, v_{cp}, v'_o in mode 1 are derived as (1)~(6) and the terms containing $i_r(t_0)$ disappear in DCM I since $i_r(t_0) = 0$.

$$i_r(t) = \frac{V_i - v_{cs}(t_0) - v_{cp}(t)}{Z_1}\sin\omega_1(t-t_0) + i_r(t_0)\cos\omega_1(t-t_0) \quad (1)$$

where $Z_1 = \sqrt{L/C_{spo}}, \omega_1 = 1/\sqrt{LC_{spo}}, L = L_r + L_{lk}$

$$C_{spo} = C_s(C_p + C'_o)/(C_s + C_p + C'_o), C_{po} = C_p + C'_o, C'_o = n^2 C_o$$

$$v_{cs}(t) = v_{cs}(t_0) + \frac{1}{\omega_1 C_s}\left[\frac{V_i - v_{Cs}(t_0) - v_{cp}(t_0)}{Z_1}(1-\cos\omega_1(t-t_0)) + i_r(t_0)\sin\omega_1(t-t_0)\right] \quad (2)$$

$$v_{cp}(t) = v_{cp}(t_0) + \frac{1}{\omega_1 C_{po}}\left[\frac{V_i - v_{cs}(t_0) - v_{cp}(t_0)}{Z_1}(1-\cos\omega_1(t-t_0)) + i_r(t_0)\sin\omega_1(t-t_0)\right] \quad (3)$$

$$i_{cp}(t) = (C_p / C_{po}) i_r(t) \quad (4)$$

$$i'_o(t) = (C'_o / C_{po}) i_r(t) \quad (5)$$

$$v'_o(t) = v_{cp}(t) \quad (6)$$

In *Mode 2* [t_1-t_2], the characteristic impedance of mode 1, Z_1 is changed to Z_2. The reversed resonant current i_r (= i_{cp}) makes D_1 and D_2 conductive. A negative i_r (= i_{cp}) flows. v_{cs} decreases and v_{cp} decreases until the absolute value of $v_{cp}(t_2)$ is equal to $v_{cp}(t_1)$. Since D_5~ D_8 are not conductive, i'_o does not flow, and v'_o is constant. The terms containing $i_r(t_1)$ disappear in both DCM I and CCM I since $i_r(t_1)$= 0. The currents i_r, i_{cp}, i'_o and the voltages v_{cs}, v_{cp}, v'_o in mode 2 are derived as (7)~(12).

$$i_r(t) = \frac{V_i - v_{cs}(t_1) - v_{cp}}{Z_2}\sin\omega_2(t-t_1) \quad (7)$$

where $Z_2 = \sqrt{L/C_{sp}}, \omega_2 = 1/\sqrt{LC_{sp}}, C_{sp} = C_s C_p/(C_s + C_p)$

$$v_{cs}(t) = v_{cs}(t_1) + \frac{1}{\omega_2 C_s}\left[\frac{V_i - v_{cs}(t_1) - v_{cp}(t_1)}{Z_2}(1-\cos\omega_2(t-t_1)\right] \quad (8)$$

$$v_{cp}(t) = v_{cp}(t_1) + \frac{1}{\omega_2 C_p}\left[\frac{V_i - v_{cs}(t_1) - v_{cp}(t_1)}{Z_2}(1-\cos\omega_2(t-t_1)\right] \quad (9)$$

$$i_{cp}(t) = i_r(t) \quad (10)$$

$$i'_o(t) = 0 \quad (11)$$

$$v'_o(t) = v_{cp}(t_1) \quad (12)$$

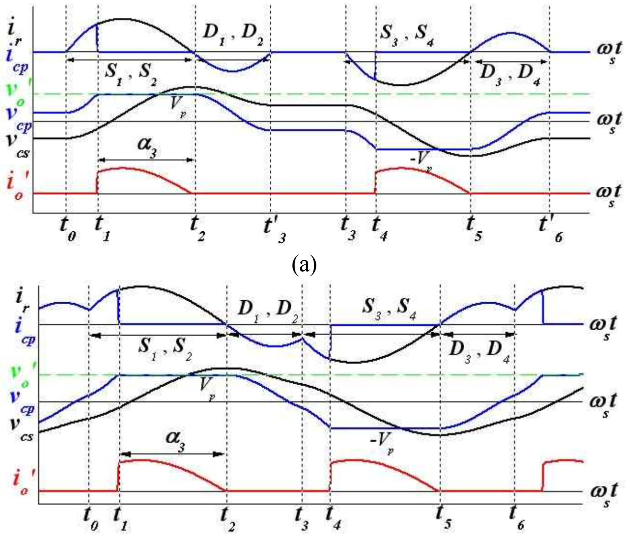

(a)

(b)

Fig. 5. Ideal waveforms of proposed capacitor charger. (a) DCM II. (b) CCM II.

In *Mode 3* [t_2-t_3], the value of $|v_{Cp}(t_2)|$ is equal to $v_{cp}(t_1)$ at $t=t_2$. D_7 and D_8 are conductive. The primary side is connected to the secondary side like mode 1. A negative i_r is divided into a negative i_{cp} and a positive i'_o. i_{cp} reversely charges C_p, and i'_o charges C'_o again. Mode 3 in DCM I is finished when D_1 and D_2 are naturally non-conductive but mode 3 in CCM I is finished when S_3 and S_4 are forcedly conductive at $t = t_3$. Actually, DCM I is divided into eight operation modes and there exist two modes where all of the switches and diodes are not conductive as shown in Fig. 3 (a). The currents i_r, i_{cp}, i'_o and the voltages v_{cs}, v_{cp}, v'_o in mode 3 are derived as (13)~(18).

$$i_r(t) = \frac{V_i - v_{cs}(t_2) - v_{cp}(t_2)}{Z_1}\sin\omega_1(t-t_2) + i_r(t_2)\cos\omega_1(t-t_2) \quad (13)$$

$$v_{cs}(t) = v_{cs}(t_2) + \frac{1}{\omega_1 C_s}\left[\frac{V_i - v_{cs}(t_2) - v_{cp}(t_2)}{Z_1}(1-\cos\omega_1(t-t_2)) + i_r(t_2)\sin\omega_1(t-t_2)\right] \quad (14)$$

$$v_{cp}(t) = v_{cp}(t_2) + \frac{1}{\omega_1 C_{po}}\left[\frac{V_i - v_{cs}(t_2) - v_{cp}(t_2)}{Z_1}(1-\cos\omega_1(t-t_2)) + i_r(t_2)\sin\omega_1(t-t_2)\right] \quad (15)$$

$$i_{cp}(t) = (C_p / C_{po}) i_r(t) \quad (16)$$

$$i'_o(t) = (C'_o / C_{po}) i_r(t) \quad (17)$$

$$v'_o(t) = -v_{cp}(t) \quad (18)$$

In the same manner, the currents and voltages for the t_3~ t_6 sections can be derived using the equivalent circuit shown in Fig. 4 (d)(e)(f).

B. Principles of Operation in DCM II and CCM II

Fig. 5 (a) and (b) show ideal waveforms in DCM II and in CCM II. Fig. 6 shows the equivalent circuits for the six

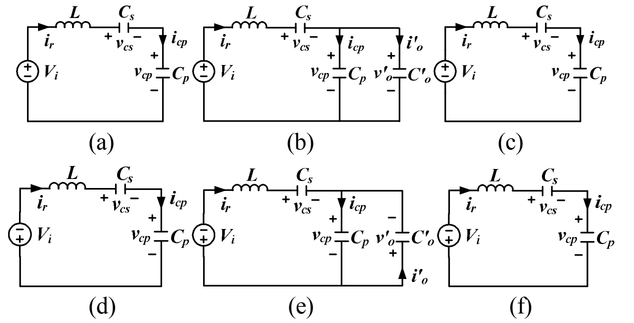

Fig. 6. Common equivalent circuit of DCM II and CCM II. (a) Mode 1. (b) Mode 2. (c) Mode 3. (d) Mode 4. (e) Mode 5. (f) Mode 6.

operation modes which commonly appear in DCM II and CCM II.

In *Mode 1* [t_0-t_1], S_1 and S_2 are conductive, a positive resonant current i_r charges C_s biased reversely, and v_{cs} increases. i_{cp} (= i_r) charges C_p and v_{cp} increase until v_{cp} is equal to v'_o at $t = t_2$. Since $D_5 \sim D_8$ are not conductive, i_o does not flow, and v'_o holds $v'_o(t_0)$. Mode 1 is finished when $v_{cp}(t_1)$ is equal to $v'_o(t)$ at $t = t_1$. The currents i_r, i_{cp}, i'_o and the voltages v_{Cs}, v_{Cp}, v'_o in mode 1 are derived as (19)~(24) and the terms containing $i_r(t_0)$ disappear in DCM II since $i_r(t_0)$= 0.

$$i_r(t) = \frac{V_i - v_{cs}(t_0) - v_{cp}(t_0)}{Z_2}\sin\omega_2(t-t_0) + i_r(t_0)\cos\omega_2(t-t_0) \quad (19)$$

$$v_{cs}(t) = v_{cs}(t_0) + \frac{1}{\omega_2 C_s}[\frac{V_i - v_{cs}(t_0) - v_{cp}(t_0)}{Z_2}(1-\cos\omega_2(t-t_0)) + i_r(t_0)\sin\omega_2(t-t_0)] \quad (20)$$

$$v_{cp}(t) = v_{cp}(t_0) + \frac{1}{\omega_2 C_p}[\frac{V_i - v_{cs}(t_0) - v_{cp}(t_0)}{Z_2}(1-\cos\omega_2(t-t_0)) + i_r(t_0)\sin\omega_2(t-t_0)] \quad (21)$$

$$i_{cp}(t) = i_r(t) \quad (22)$$

$$i_o^{'}(t) = 0 \quad (23)$$

$$v_o^{'}(t) = v_{cp}(t_1) \quad (24)$$

In *Mode 2* [t_1-t_2], the characteristic impedance of mode 1, Z_2 is changed to Z_1. D_5 and D_6 are conductive. The primary side is connected to the secondary side. i_r is divided into i_{cp} and i'_o. A positive i_r charges C_s, and v_{cs} continuously increases. A relatively small i_{cp} charges C_p, and i'_o charges C'_o. v_{cp} (= v'_o) increases by a very small amount. The currents i_r, i_{cp}, i'_o and the voltages v_{Cs}, v_{Cp}, v'_o in mode 2 are derived as (25)~(30).

$$i_r(t) = \frac{V_i - v_{cs}(t_1) - v_{cp}(t_1)}{Z_1}\sin\omega_1(t-t_1) + i_r(t_1)\cos\omega_1(t-t_1) \quad (25)$$

$$v_{cs}(t) = v_{cs}(t_1) + \frac{1}{\omega_1 C_s}[\frac{V_i - v_{cs}(t_1) - v_{cp}(t_1)}{Z_1}(1-\cos\omega_1(t-t_1)) + i_r(t_1)\sin\omega_1(t-t_1)] \quad (26)$$

$$v_{cp}(t) = v_{cp}(t_1) + \frac{1}{\omega_1 C_{po}}[\frac{V_i - v_{cs}(t_1) - v_{cp}(t_1)}{Z_1}(1-\cos\omega_1(t-t_1)) \quad (27)$$

$$i_{cp}(t) = (C_p / C_{po}) i_r(t) \quad (28)$$

$$i_o^{'}(t) = (C_o^{'} / C_{po}) i_r(t) \quad (29)$$

$$v_o^{'}(t) = v_{cp}(t) \quad (30)$$

In *Mode 3* [t_2-t_3], the characteristic impedance of mode 2, Z_1 is again changed to Z_2. At $t = t_2$, the resonant current is reversed, and D_1 and D_2 are conductive. Because $v_{cp}(t)$ is less than $v'_o(t)$, D_5 and D_6 are not conductive, and the primary side is separated from the secondary side. i_r (=i_{cp}) is circulating through C_p, and i'_o does not flow. S_1 and S_2 are naturally conductive at $t = t_2$ and zero current switching (ZCS) is achieved. Mode 3 in DCM II is finished when D_1 and D_2 are naturally non-conductive. However, mode 3 in CCM II is finished when S_3 and S_4 are forcedly conductive at $t = t_3$. The terms containing $i_r(t_2)$ disappear in both DCM II and CCM II since $i_r(t_2)$=0. The currents i_r, i_{cp}, i'_o and the voltages v_{Cs}, v_{Cp}, v'_o in mode 3 are derived as (31)~(36).

$$i_r(t) = \frac{V_i - v_{Cs}(t_2) - v_{cp}(t_2)}{Z_2}\sin\omega_2(t-t_2) \quad (31)$$

$$v_{cs}(t) = v_{cs}(t_2) + \frac{1}{\omega_2 C_s}[\frac{V_i - v_{cs}(t_2) - v_{cp}(t_2)}{Z_2}(1-\cos\omega_2(t-t_2))] \quad (32)$$

$$v_{cp}(t) = v_{cp}(t_2) + \frac{1}{\omega_2 C_p}[\frac{V_i - v_{Cs}(t_2) - v_{cp}(t_2)}{Z_2}(1-\cos\omega_2(t-t_2))] \quad (33)$$

$$i_{cp}(t) = i_r(t) \quad (34)$$

$$i_o^{'}(t) = 0 \quad (35)$$

$$v_o^{'}(t) = v_{cp}(t_2) \quad (36)$$

In the same manner, the currents and voltages for the $t_3 \sim t_6$ sections can be derived using the equivalent circuit shown in Fig .6 (d)(e)(f).

C. Mode Changes by Switching Frequency Section

As shown in Fig. 2, when the proposed capacitor charger is operated in the range of switching frequency below the resonant frequency, the operational modes are changed differently by the four switching frequency sections as the output voltage increases.

Section I [ω_s<$0.5\omega_1$]: Below boundary line 1, this capacitor charger operates in DCM I. γ_1=0 at v'_o=0. As v'_o increases, γ_1 also increases, and δ_1 reduces. δ_1=0 at v'_o= v'_{oBND}. Above boundary line 1, this capacitor charger operates in DCM II. As v'_o increases, α_3 gradually decreases.

Section II [$0.5\omega_1$<ω_s<ω_{sBND1}]: This capacitor charger initially operates in CCM I since ω_s>$0.5\omega_1$. As v'_o increases, α_2 and γ_2 increase, and δ_2 reduces. After i_r = 0 at $t = t_0$ and $t = t_3$ (boundary line 2), this capacitor charger operates in DCM I. The following operation is equal to section I [ω_s<$0.5\omega_1$]. DCM I changes to DCM II at v'_o= v'_{oBND}.

Section III [ω_{sBND1}<ω_s<ω_{sBND2}]: This capacitor charger initially operates in CCM I since ω_s>$0.5\omega_1$ in common with section II. As v'_o increases, α_2 and γ_2 increase, and δ_2 reduces. At v'_o= v'_{oBND}, δ_2=0, and CCM I changes to CCM II. As v'_o continues to increase, CCM II changes to DCM II at boundary line 2.

Section IV [$\omega_{sBND2}<\omega_s<\omega_1$]: Section IV is similar to section III but DCM II does not appear in the end of charging because the value of ω_s/ω_1 is relatively large. Above boundary line 1, α_4 gradually decreases as v'_o continues to increase.

D. Nonlinearity of the Average Charging Current

In this capacitor charger, the output capacitor is an energy storage capacitor, and the capacitance C_o is usually at the mF level. As a result, the transformer stray capacitance is much smaller than the output capacitance which is converted to the primary side ($C_p<<C'_o$) and the parallel resonant current is much smaller than series resonant current ($i_{cp}<<i_r$) in mode 1 and mode 3 of DCM I and DCM II. Thus (5) and (17) can be approximated to (37). Equation (3) and (15) can also be approximated to (38).

$$i'_o(t)=i_r(t) \tag{37}$$

$$v_{cp}(t)=\pm V_p \tag{38}$$

Using (1) and (13), the average charging current, which is converted to the primary side during a half period I'_o in DCM I, is derived as (39) and I'_o in CCM I is derived as (40).

$$I'_o=\frac{m_{sp}}{\pi}\Big[\frac{V_i-v_{cs}(t_2)+V_p}{Z_1}\cos\delta_1-i_r(t_2)\sin\delta_1+\frac{V_i-2v_{cs}(t_0)+v_{cs}(t_2)-3V_p}{Z_1}\Big] \tag{39}$$

where $m_{sp}=\omega_s/\omega_1,\ \delta_1=\pi-\tan^{-1}\left(\frac{i_r(t_2)Z_1}{V_i-v_{cs}(t_2)+V_p}\right)\ or\ =-\tan^{-1}\left(\frac{i_r(t_2)Z_1}{V_i-v_{cs}(t_2)+V_p}\right)[rad]$

$$I'_o=\frac{m_{sp}}{\pi}\Big[\frac{V_p+v_{cs}(t_0)-V_i}{Z_1}\cos\alpha_2+\frac{V_i-v_{cs}(t_2)+V_p}{Z_1}\cos\delta_2+i_r(t_0)\sin\alpha_2-i_r(t_2)\sin\delta_2+\frac{v_{cs}(t_2)-v_{cs}(t_0)-2V_p}{Z_1}\Big] \tag{40}$$

where
$$\alpha_2=\pi-\tan^{-1}\left(\frac{i_r(t_0)Z_1}{V_i-v_{cs}(t_0)+V_p}\right)[rad],$$
$$\gamma_2=\cos^{-1}\left(1+\frac{2V_p(1+C_p/C_s)}{V_i-V_{cs}(t_1)-V_p}\right)[rad],$$
$$\delta_2=\pi+\sin^{-1}\left(\frac{C}{\sqrt{A^2+B^2}}\right)-\tan^{-1}\left(\frac{B}{A}\right)or=\sin^{-1}\left(\frac{C}{\sqrt{A^2+B^2}}\right)-\tan^{-1}\left(\frac{B}{A}\right),$$
$$A=\frac{V_i-v_{cs}(t_2)+V_p}{Z_1},B=\frac{V_i-v_{cs}(t_1)-V_p}{Z_2}\sin\gamma_2,C=\frac{V_i-v_{cs}(t_0)-V_p}{Z_1}\tan\alpha_2$$

$$I'_o=\frac{m_{sp}}{\pi}\Big[\frac{V_p+v_{cs}(t_1)-V_i}{Z_1}\cos\alpha_3+i_r(t_1)\sin\alpha_3+\frac{V_i-v_{cs}(t_1)-V_p}{Z_1}\Big] \tag{41}$$

If the same rule ($C_p<<C'_o$, $i_{cp}<<i_r$) is applied to mode 2 of DCM II and CCM II, (29) and (27) can each be approximated to (37) and (38). Using (25), I'_o in DCM II and CCM II is commonly derived as (41).

TABLE I

SPECIFICATIONS OF CAPACITOR CHARGER

Parameter	Value	Parameter	Value
V_i [V]	300	n	11
V_o [V]	3300	f_s [kHz]	20~32
V_T [V]	3000	t_c [s] at $\omega_s=0.5\omega_1$	4.6
C_o [μF]	16.4	V_B [V]	300
C_s [μF]	0.243	I_B (=V_B/Z_1) [A]	18.34
C_p [μF]	0.1C_s ~0.5C_s	P_B (=V_BI_B) [W]	5502
L [μH]	65	t_B [s]	10

where $\alpha_3=\pi-\tan^{-1}\left(\frac{i_r(t_1)Z_1}{V_i-v_{cs}(t_1)-V_p}\right)\ or\ =\tan^{-1}\left(-\frac{i_r(t_1)Z_1}{V_i-v_{cs}(t_1)-V_p}\right)$

When an ideal series resonant type capacitor charger which is not considering the transformer stray capacitance is operated in DCM ($\omega_s<0.5\omega_r$), I'_o is constant as (42), and the charging time t_c can be easily derived using (43) [15].

$$I'_o=\frac{m_s}{\pi}\cdot\frac{4V_i}{Z_r} \tag{42}$$

$$t_c=\frac{C_oV_o}{I_o}=\frac{nC_oV_o}{I'_o} \tag{43}$$

However, in a capacitor charger considering the transformer stray capacitance, I'_o is not constant in each operation mode such as (39), (40), and (41) because $i_r(t_x)$, $v_{cs}(t_x)$, V_p, α_y, γ_y, and δ_y (where x=0~2 and y=1~4) are continuously changed as the output voltage increases. Thus it is very difficult to calculate an accurate charging time mathematically since I'_o appears in combination with the four switching frequency sections (section I ~ section IV). Because of this nonlinearity of I'_o, several parameters including the charging time are calculated by a simulation tool (PSIM software) in this paper.

III. SIMULATION OF CHARGING CHARACTERISTICS

Table I shows the specifications which are established for the experiment. In this capacitor charger, C_{po}(=C'_o+C_p) is connected to C_s in series so that the equivalent capacitance C_{spo} and the system characteristic impedance Z_1 are nearly not changed even if C_o becomes smaller than the original C_o. Thus C_o is set to 16.4 μF which is reduced by one hundredth the experimental value 1640 μF to shorten the simulation time. Fig. 7 shows the currents i_r, i_{cp}, and i_o as the output voltage increases under the conditions of ω_s= 0.6ω_1 and k = 0.1. This capacitor charger operates in CCM I at v'_o/V_i= 0.2. After that, it operates in DCM I at v'_o/V_i= 0.8 and in DCM II at v'_o/V_i= 1.0. That is, this capacitor charger has an ideal series resonant characteristic in the early stage of charging because the conduction period (γ_2) of i_{cp} is relatively short. However, it has a series-parallel resonant characteristic as the output voltage increases because the peak value and conduction period (γ_1, γ_2) of i_{cp} gradually increase. Fig. 8 shows the normalized peak resonant current i_{rpeakN}(=i_{rpeak}/I_B) and voltage $v_{cspeakN}$(=v_{cspeak}/V_B) as the switching frequency, output voltage, and k value are changed. As the k value and v'_o increase, i_{rpeakN} and $v_{cspeakN}$ totally decrease. From this effect, the rated current and voltage of the main switch, resonant component, and transformer are advantageously reduced. However, the average charging current is reduced so that the charging time t_c to reach the target voltage V_T disadvantageously increases. Fig. 9 shows the v'_o curves according to the changes of the k value. As the k value increases, the DPC section decreases and the SPC section increases. As a result, t_c increases. In addition, if V_T is set up as low as possible when compared with V_o, t_c decreases. For example, t_c is smaller in $V_T = V_{T1}$ than it is in $V_T= V_{T2}$. The smaller C_p of the transformer (or k value) is, the larger the average charging current and the larger the amount of charge which is charged to the load capacitor become. The larger the average charging current is, the smaller the charging time t_c is. Therefore, the charging power expressed as (44) increases and the performance of the repetition rate of this capacitor charger is improved. When the C_p value (or k value) is equal to zero ultimately, the charger has an ideal series resonant charging characteristic.

$$P_{CH} = \frac{0.5C_oV_o}{t_c} \tag{44}$$

Consequently, two design rules to get good performance from this series resonant capacitor charger are:

1) Design a transformer whose stray capacitance C_p is minimized.
2) Set the target voltage V_T as low as possible when compared with the output voltage V_o.

IV. EXPERIMENTAL RESULTS

To verify the results of the analysis and simulation, a prototype capacitor charger (1.8 kJ/s at ω_s/ω_1=0.5) is constructed by using the specification that are outlined in Table I, as shown in Fig.10. A 40 kJ, 7 kV, and 1640 µF capacitor (ICAR) is used as the load capacitor and a 28335 TI 32 bit floating point processor controller is used for generating the switching signal. Fig.11 show the voltage and current waveforms at f_s=24 kHz (ω_s/ω_1=0.6). It has been verified that CCM I, DCM I and DCM II appear sequentially as the output voltage increases through the (a), (b) and (c) waveforms. This experimental result is an example of "*Section II*" of "*C. Mode Changes by Switching Frequency Section*" in chapter II. To examine the relation between C_p and t_c, two transformers whose C_p values are different are tested in terms of t_c. Table II shows the parameters of two transformers (T1 and T2) which are dissimilarly designed and manufactured. Fig. 12 shows photographs, longitudinal sections, and equivalent circuits of the secondary winding of

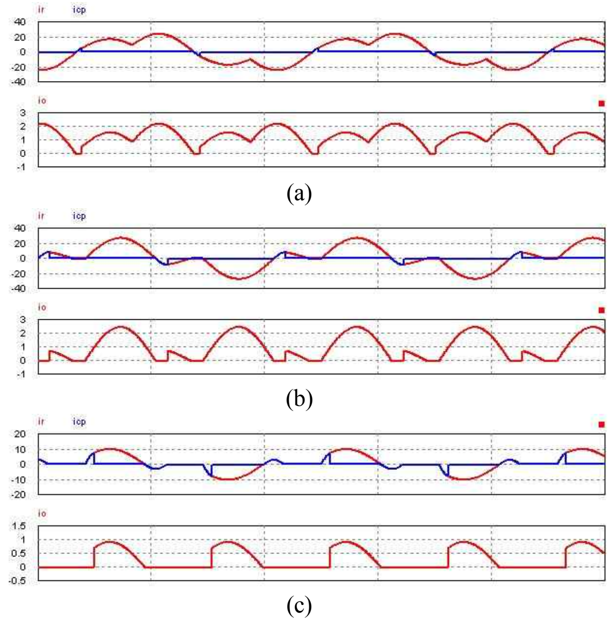

Fig. 7. i_r, i_{cp}, i_o [*x-axis*: 20 µs/div]. (a) v'_o/V_i=0.2. (b) v'_o/V_i=0.8. (c) v'_o/V_i=1.

T1 and T2. The charging time t_c increases about 18% in the experimental result by using T1 when compared with the simulation result using an ideal transformer. For this reason, T2 was manufactured by three different method as follows to minimize the parallel stray capacitance [16]. Firstly, the layer insulation thickness of the secondary winding was increased. As shown in Fig. 12, D_1 is the layer insulation thickness of the secondary winding of T1, and D_2 is the layer insulation thickness of the secondary winding of T2. Here, D_1 is smaller than D_2. Secondly, the winding width of the secondary winding was decreased. A_1 is the winding width of the secondary winding of T1, and A_2 is the winding width of the secondary winding of T2. Here, A_1 is larger than A_2. Thirdly, the layer number of the secondary winding was increased. The layer number of the secondary winding of T1 is 6, and the layer number of the secondary winding of T2 is 7. As the layer number increases, the series connection number of the layer to layer capacitance (C_1 or C_2) increases, and the total stray capacitance (C_W) decreases. It other words, C_{W2} is smaller than C_{W1}. Fig.13 shows the voltage and current waveforms during the total charging period by using T1 (C_p=0.034 µF, k=0.14) and T2 (C_p=0.023 µF, k=0.095) at f_s=20 kHz, respectively. The charging times taken to reach V_T =3 kV are 5.46 s and 5.11 s which are increased by 18 % and 10 % in comparison with the expecting time (4.6 s) with the ideal transformer (k=0, C_p=0). Table III and Fig.14 show the experimental and simulation results of t_c according to variations of the k value in the range of 16~26 kHz. It has been verified that a small transformer stray capacitance reduces the charging time, and improves the performance of the capacitor charger.

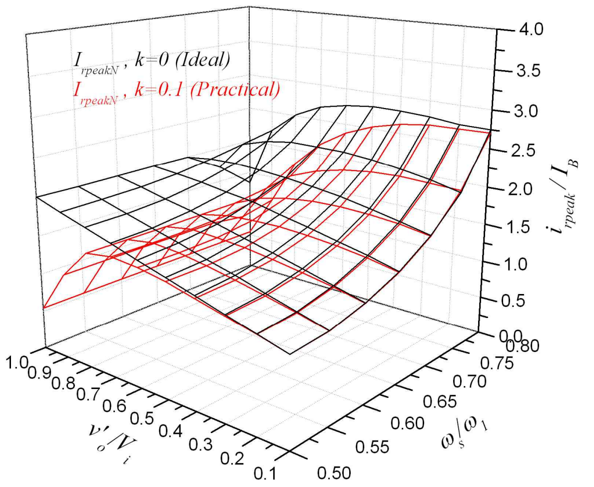

(a)

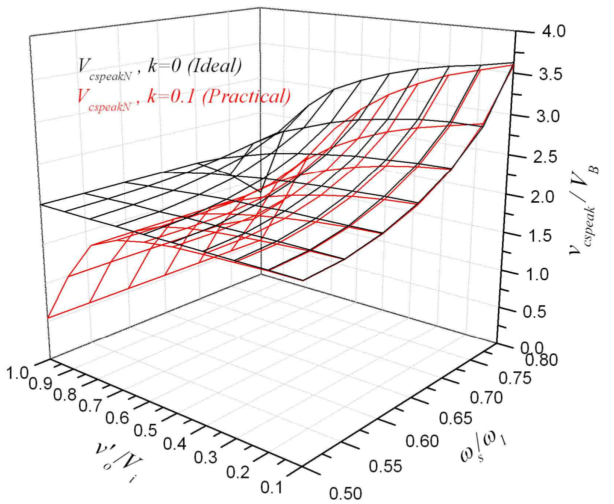

(b)

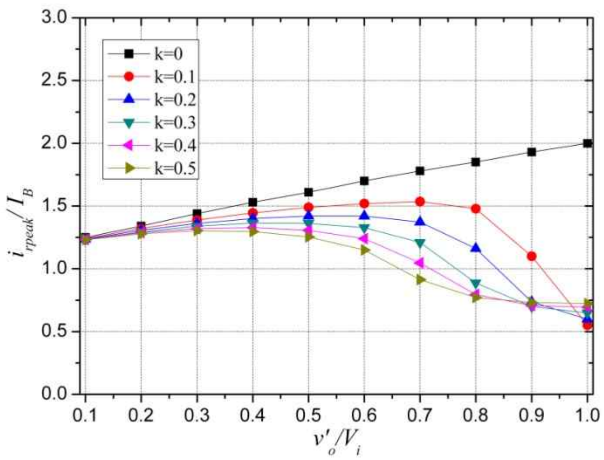

(c)

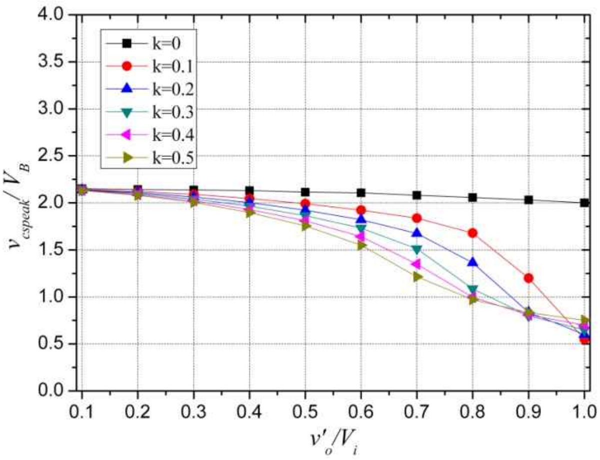

(d)

Fig. 8. Normalized current and voltage versus k value variation. (a) i_{rpeak}/I_B. (b) v_{cspeak}/V_B. (c) i_{rpeak}/I_B (at $\omega_s/\omega_1 = 0.6$). (d) v_{cspeak}/V_B (at $\omega_s/\omega_1 = 0.6$).

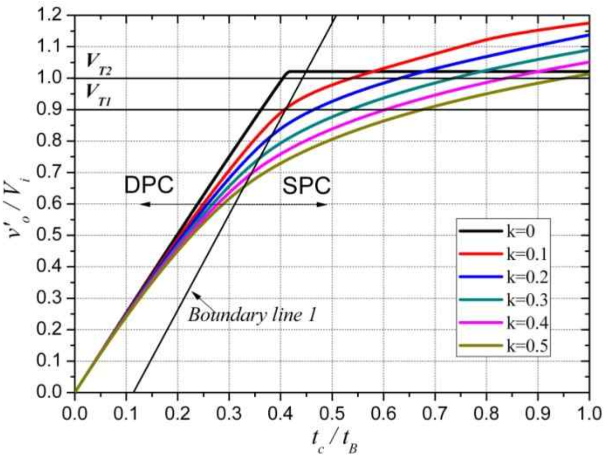

Fig. 9. v'_o/V_i and t_c/t_B versus k value variation at ω_s/ω_1=0.6.

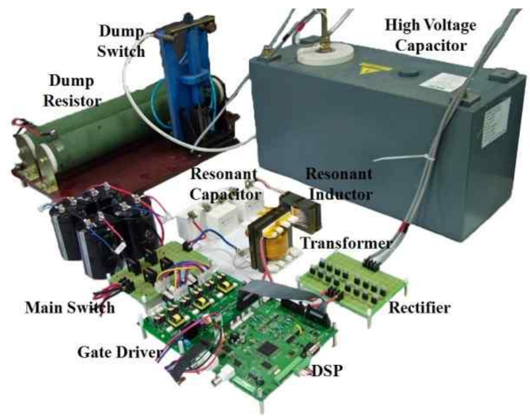

Fig. 10. 1.8 kJ/s prototype charger with 40 kJ capacitor load.

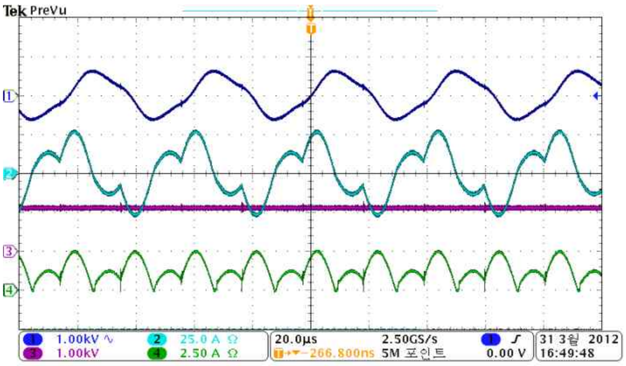

(a)

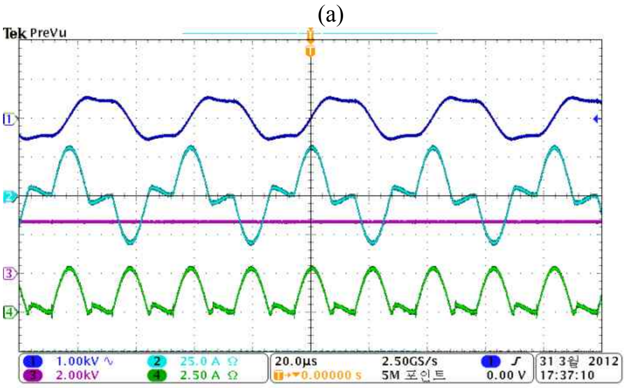

(b)

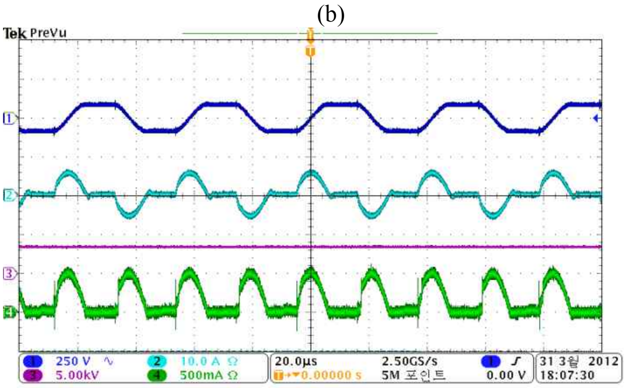

(c)

Fig. 11. Voltage and current waveforms (CH1:v_{cs} CH2:i_r CH3:v_o CH4:i_o). (a) v_o= 1.1 kV. (b) v_o= 2.6 kV. (c) v_o= 3.3 kV.

TABLE II

COMPARISON OF TWO TRANSFORMERS' PARAMETER

Parameter	**Transformer1 (T1)**	**Transformer2 (T2)**
Designed B_{max} [T]	0.2	0.25
Primary : Secondary [turn]	29 : 319	23 : 253
Primary winding layer number	2	1
Secondary winding layer number	6	7
C_p [μF]	0.034	0.023
L_{lk} [μH]	14.6	9.17

TABLE III

CHARGING TIME (EXPERIMENTAL RESULT)

ω_s / ω_1	f_s [kHz]	t_c [s] (T1, k=0.14)	t_c [s] (T2, k=0.095)
0.4	16	6.78	6.36
0.45	18	6.18	5.68
0.5	20	5.46	5.11
0.55	22	5.06	4.56
0.6	24	4.62	4.11
0.65	26	4.42	3.80

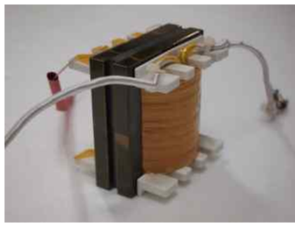

(a)

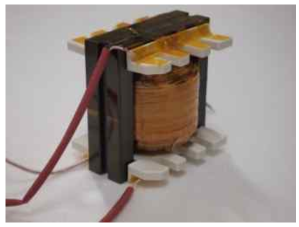

(b)

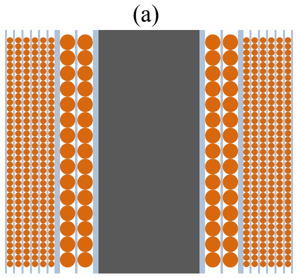

(c)

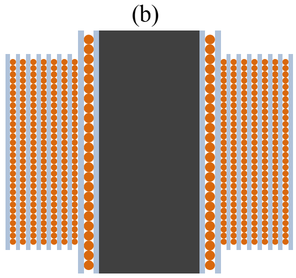

(d)

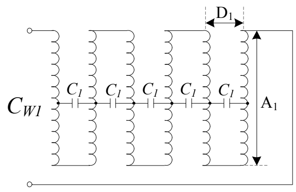

(e)

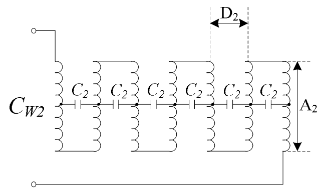

(f)

Fig.12. Comparison of the transformer1 (T1) and transformer2 (T2). (a) Photograph of T1. (b) Photograph of T2. (c) Longitudinal section of T1. (d) Longitudinal section of T2. (e) Equivalent circuit of secondary winding of T1. (f) Equivalent circuit of secondary winding of T2.

V. CONCLUSIONS

In this paper, a series resonant type high voltage capacitor charger considering the transformer stray capacitance has been studied. The operating equations of this capacitor charger have been derived and analyzed in the range of switching frequencies below the resonant frequency. Four operational modes (DCM I, CCM I, DCM II, and CCM II) are combined by the four operating frequency sections ($\omega_s<0.5\omega_1$, $0.5\omega_1<\omega_s<\omega_{sBND1}$, $\omega_{sBND1}<\omega_s<\omega_{sBND2}$, and $\omega_{sBND2}<\omega_s<\omega_1$) as the output voltage increases. The following features has been confirmed in this capacitor charger. First, each average charging current for the four operational modes has a nonlinear characteristic as the output voltage increases. Second, it is possible to minimize the rated voltage and

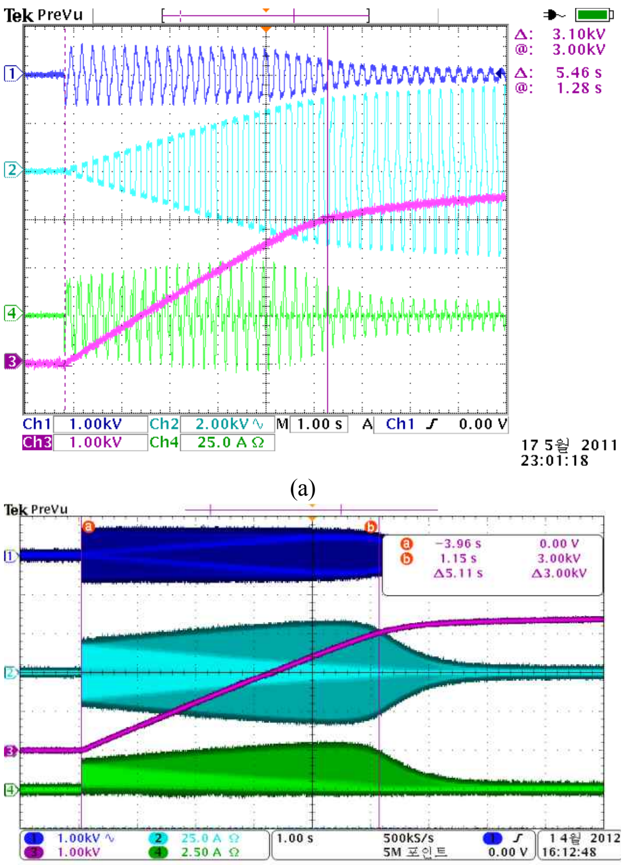

(b)

Fig. 13. Voltage and current waveforms (a) k=0.14 (CH1:v_{cs} CH2:v_{sec} CH3:v_o CH4:i_r). (b) k=0.095 (CH1:v_{cs} CH2:i_r CH3:v_o CH4:i_o).

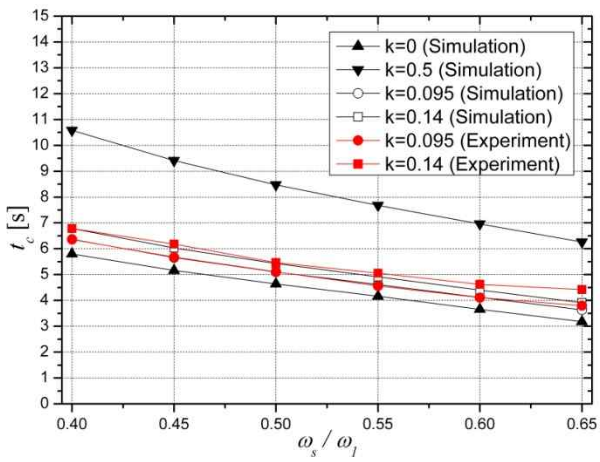

Fig. 14. Charging time (t_c versus ω_s / ω_I).

current of the main components because the resonant peak current and voltage decrease as the transformer stray capacitance increases. Third, an increase of the stray capacitance causes a decreases of the average charging current and charging time. A 1.8 kJ/s prototype capacitor charger was constructed. The analysis and simulation results considering the transformer stray capacitance were verified by the experiment.

ACKNOWLEDGMENT

This work was supported by the Human Resources Development of the Korea Institute of Energy Technology Evaluation and Planning (KETEP) grant funded by Korea government Ministry of Knowledge Economy (No.2012-4030200090).

REFERENCES

[1] I. R. McNab, F. Stefani, M. Crawford, M. Eregnil, C. Persad, S. Satapathy, H. Vanicek, T. Watt, and C. Dampier, “Development of a naval railgun,” *IEEE Trans. Magn.*, Vol. 41, No. 1, pp. 206-210, Jan. 2005.

[2] M. Del Guercio, “A 4.5-MJ pulsed power supply for railgun experiments,” *IEEE Trans. Magn.*, Vol. 39, No. 1, pp. 280-284, Jan. 2003.

[3] T. Wolfe, P. Riedy, J. Drake, F. MacDougall, and J. Bernardes, “Preliminary design of a 200 MJ pulsed power system for a naval railgun proof of concept facility,” *in Proc. 15th International Pulsed Power Conf.*, pp. 70-74, 2005.

[4] J. M. Neri and B. M. Human, “Operation of a 5-MJ capacitor bank for EML materials testing,” *in Proc. 16th International Pulsed Power Conf.*, pp. 1736-1739, 2007.

[5] G. Ortiz, D. Bortis, J. Biela, and J. W. Kolar, “Optimal design of a 3.5 kV/11 kW DC-DC converter for charging capacitor banks of power modulators,” *IEEE Trans. Plasma Sci.*, Vol. 38, No. 10, pp. 2565-2573, Oct. 2010.

[6] S.-H. Kim, B.-S. Kim, Y.-D. Lee, B.-K. Kwon, J.-S. Kim, C.-H. Choi, and S.-G. Choi, “A new capacitor charging power supply using phase-shifted PWM full-bridge converter,” in *Proc. IEEE-ECCE*, pp. 490-494, 2009.

[7] H. Sheng, W Shen, H. Wang, D. Fu, Y. Pei, X. Yang, F. Wang, D. Boroyevich, F. C. Lee, and C. W. Tipton, “Design and implementation of a high power density three-level parallel resonant converter for capacitor charging pulsed-power supply,” *IEEE Trans. Plasma Sci.*, Vol. 39, No. 4, pp. 1131-1140, Apr. 2011.

[8] M. Borage, S. Tiwari, and S. Kotaiah, “Constant-current, constant- voltage half-bridge resonant power supply for capacitor charging,” *IEE Electr. Power. Appl.*, Vol. 153, No. 3, pp. 343-347, May 2006.

[9] Q. Tan, F. Lin, S. Wang, H. Zhong, G. Liu, and Y. Deng, “Improved capacitor charging power supply for a power conditioning system,” *IEEE Trans. Dielectr. Electr. Insul.*, Vol. 18, No. 4, pp.1214- 1220, Aug. 2011.

[10] Z. Zhang, Q. Liu, Z. Wu, Q. Wang and H. Yang, “Design and implementation of HF AC-link capacitor charging power supply,” in *Proc. AIMSEC*, pp. 3856-3859, 2011.

[11] Y. Gao, Y. Sun, P. Yan, and Y. Shi, “High power capacitor charging power supply for EML applications,” *in Proc. 14th Electromagnetic Launch Technology Sympos.*, pp. 10-18, 2008.

[12] A. K. Jain, C. P. Henze, C. B. Henze and K. Conroy, “Development of a 350kW,10kV pulse power converter for capacitor charging,” in *Proc. IEEE-APEC.*, pp. 1164-1170, 2007.

[13] I. W. Jung, J. S. Kim, G. I. Gusev, and G. H. Rim, "Design of 35 kJ/s 25 kV capacitor charging power supply for pulsed power system," in *Proc. IEEE-IECON*, pp. 2860-2863, 2004.
[14] A. C. Lippincott and R. M. Nelms, "A capacitor-charging power supply using a series-resonant topology, constant on-time/variable frequency control, and zero-current switching," *IEEE Trans. Ind. Electr.* Vol. 38, No. 6, pp. 438-447, Dec. 1991.
[15] B. Lee and H. Cha, "Comparative analysis of charging mode of series resonant converter for a energy storage capacitor," *in Proc. IEEE-APEC*, pp. 2200-2205, Feb. 2012.
[16] Colonel Wm. T. McLyman, *Transformer and Inductor Design Handbook*, 2nd ed., Marcel Dekker, Inc. New York, chap. 6, 1988.

Byungha Lee received his B.S. and M.S. in Electrical Engineering from Chungnam National University, Daejeon, Korea, in 1994 and 1996, respectively, where, he is currently working toward his Ph.D. in Electrical Engineering. Since 1996, he has been a Senior Researcher with Agency for Defense Development, Daejeon, Korea. His current research interests include military pulsed-power systems and electromagnetic launch technologies.

Hanju Cha received his B.S. in Electrical Engineering from Seoul National University, Seoul, Korea, in 1988, his M.S. in Electrical Engineering from the Pohang Institute of Science and Technology, Pohang, Korea, in 1990, and his Ph.D. in Electrical Engineering from Texas A&M University, College Station, TX, USA, in 2004. From 1990 to 2001, he was with LG Industrial Systems, Anyang, Korea, where he was engaged in the development of power electronics and adjustable speed drives. Since 2005, he has been with the Department of Electrical Engineering, Chungnam National University, Daejeon, Korea. He was a Visiting Professor at the United Technology Research Center, Hartford, CT, USA, in 2009. His current research interests include high-power converters, ac/dc, dc/ac, and ac/ac converter topologies, power quality, and utility interface issues for distributed energy systems and micro-grids.